THREE-DIMENSIONAL, NONLINEAR, VISCOUS WAVE INTERACTIONS IN A SLOSHING TANK

Ben R. Hodges

Robert L. Street

Environmental Fluid Mechanics Laboratory
Department of Civil Engineering
Stanford University, Stanford, CA 94305-4020

ABSTRACT

A numerical simulation method for the unsteady, incompressible, Navier-Stokes equations applied to viscous free-surface flows has been developed and tested on three-dimensional (3D) and two-dimensional (2D) nonlinear, finite-amplitude standing waves in a rectangular domain. Results are presented for a 3D simulation of two monochromatic waves that are initially superposed at a 90 degree angle. A comparison of 3D simulation results with 2D results provides a basis for analyzing nonlinear wave-wave interaction effects. Viscous damping effects are compared with theory, and wave-wave interactions are analyzed by decomposing into separate nonlinear effects.

NOMENCLATURE

a	wave amplitude
d	depth
$d1$, $d2$	diagonal symmetry planes
e_{ij}	rate-of-strain tensor
g	gravity
h	wave height
k	wave number
n_j	unit normal vector
p	pressure
t_i	unit tangent vector
t	time
T	theoretical wave period
w	vertical velocity
Δ	(or delta) a portion of surface deformation attributable to nonlinear wave-wave interaction
η	(or eta) surface deformation from quiescent level
ν	kinematic viscosity
ω	wave frequency

INTRODUCTION

This is the second conference paper documenting the development of a numerical simulation code for viscous, nonlinear free-surface problems. The first paper, Hodges *et al.* (1994), provides a literature review, detailed explanation of the numerical method, and validation of the method for two-dimensional (2D) nonlinear surface waves. This paper demonstrates the ability of the method to simulate a three-dimensional (3D) free-surface problem with viscous and nonlinear effects.

NUMERICAL METHOD

Our approach has been to work with second-order accurate numerical schemes that can be implemented efficiently on a single processor of a vector machine. The foundation of our method is a non-staggered grid, finite-volume method in boundary-fitted curvilinear coordinates developed by Zang *et al.* (1994), which traces its lineage to the time-splitting method of Kim and Moin (1985). The numerical method solves the unsteady, incompressible, Navier-Stokes equations on a three-dimensional domain where the coordinates and equations in physical space are mapped into a cube in computational space. The equations in computational space are more complex, but their discretization is simplified. As the free surface moves with each time step, a new mapping is calculated so that the free surface remains coincident with a boundary in computational space. The free surface is advanced using a curvilinear space formulation of the kinematic boundary condition that does not require the wave to be single-valued in physical space (Hodges *et al.* 1994). Currently, limitations of computational memory, computational time, and the unsolved problems associated with wave-breaking prevent us from simulating multi-valued waves. Discretization of the kinematic boundary condition is through the space-implicit, time-explicit method of Chan and Street (1970). The free-surface

dynamic boundary conditions for this simulation are: (1) the zero tangential stress condition:

$$e_{ij}\, t_i\, n_j \;=\; 0 \tag{1}$$

where e_{ij} is the rate of strain tensor and t_i and n_j are the unit tangent and unit normal vectors, respectively; and (2) constant surface pressure (p):

$$p \;=\; 0 \tag{2}$$

It is planned that future simulations will include both the surface tension and surface-normal viscous effects that are neglected in equation (2).

Further details of our numerical method and two-dimensional validation simulations can be found in Hodges *et al.* (1994). Complete details of the three-dimensional method are to appear in Hodges (1996).

SIMULATION SET-UP

The problem solved is liquid sloshing in a square tank. The initial free surface position is computed from two identical standing waves that are linearly superposed at a 90 degree angle. Each individual wave is monochromatic, nonlinear, and of finite amplitude (using a second-order approximation from Wiegel, 1964). This provides the initial free surface shape shown in Figure (1). The simulation grid contains $32 \times 32 \times 32$ grid cells (for clarity, only one-quarter of the grid cells on the surface are shown). In all figures in this paper, the horizontal coordinates are non-dimensionalized by the lowest mode wavelength, while the surface deformation (η or eta, measured from still free-surface level) is non-dimensionalized by the combined amplitudes of the two superposed waves.

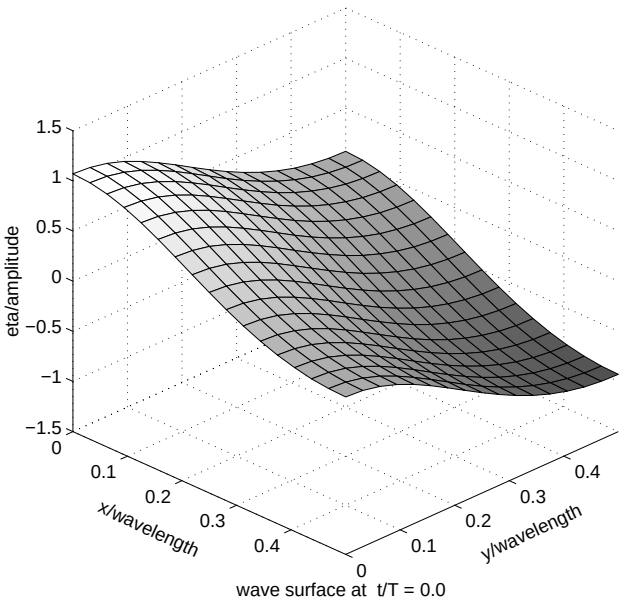

Figure 1: Superposition of two 2D waves

The simulation domain is one-half of a wavelength in length and breadth and one-tenth of a wavelength in depth ($50\,cm \times 50\,cm \times 10\,cm$). The depth of the simulation was chosen in conjunction with the viscosity of the fluid ($7.32 \times 10^{-5}\, m^2/s$) so that the free-surface boundary layer could be resolved using five grid cells without requiring excessive computational time or memory. While the viscosity is still significantly larger than that of water, it is approximately one-fifth of that used in the recent linearized free-surface simulations of Borue *et al.* (1995).

The initial velocity field is the irrotational solution at the maximum displacement of a standing wave (*i.e.* zero for all velocity components). At the start of the simulation, the upper surface is set free and is allowed to evolve in response to the nonlinear kinematic and dynamic boundary conditions as applied to the Navier-Stokes equations. Each of the superposed waves has the following initial characteristics: the wave number (k) is 6.28 $1/m$, the wave Reynolds number ($\omega/\nu\, k^2$) is approximately 2000, the wave ak is 0.0314, the wavelength is 100 cm, and the individual component wave amplitude is $0.5\,cm$. The frequency (ω) of the component waves is 5.86 rad/sec, as computed from the dispersion relation (Wiegel, 1964):

$$\omega^2 \;=\; gk\, tanh\,(kd) \tag{3}$$

where g is gravity, d is the depth, and k is the wave number.

The combination of the two waves has a sloshing amplitude of $1.0\,cm$ along a diagonal axis of $70.7\,cm$. Since the initial conditions are a linear superposition of the two waves, we expect that the primary oscillation of the system should be at the same frequency as the individual waves until the nonlinear interactions have had enough time to act upon the system. However, we should see some nonlinear effects occurring at wavelengths equal to the diagonal axis and twice the diagonal axis. These dimensions have wave k values of 8.89 $1/m$ and 4.44 $1/m$, respectively. The system ak based on the diagonal sloshing is 0.04. From the dispersion relation, we might expect nonlinear effects occurring at frequencies of 7.87 and 4.26 rad/sec, corresponding to the two primary diagonal modes.

The sidewall and bottom boundary conditions are free-slip (no boundary layer). This is appropriate for this simulation since the presence of sidewall boundary layers would obscure the free-surface viscous effects which we seek to capture.

SIMULATION RESULTS

The simulation was carried out for approximately twelve wave periods (4700 time steps). For analysis, we ran an additional simulation of viscous 2D sloshing of one of the monochromatic component waves. Both the 3D and the 2D simulations oscillated with a primary period equal to the theoretical period (for a 2D finite-amplitude standing wave) with an uncertainty of 0.25%. The uncertainty was not surprising since the wave period was not evenly divisible by the simulation time step. There was no perceptible increase or decrease of the period over the course of the simulation, so we can conclude that the duration of the

simulation was insufficient for nonlinear interactions to have any significant effect on the overall period of the sloshing. This is a reasonable result. The waves are in linear superposition to the first order, therefore it should require a relatively large number of wave periods for the higher-order nonlinear terms to have a large-scale effect on the dispersion relation.

The effect of wave-wave interactions on the surface deformation (Δ) in the 3D simulation is defined by subtracting the wave surface (η_{2D}) formed from a 90 degree superposition of two of the 2D monochromatic simulations from the wave surface of the 3D (η_{3D}) simulation:

$$\Delta^{[total]} \equiv \eta_{3D} - \eta_{2D} \tag{4}$$

Since the simulation of the 2D component wave is also nonlinear, this approach removes the nonlinear interactions of each wave with itself, leaving only the interactions between the two waves. Figure (2) shows a plot of the difference between the 3D wave and the superposition of the 2D waves after nine periods have been simulated. This is the total nonlinear effect of wave-wave interactions on the surface deformation (which we will call the "surface deformation effect"). For this point in time ($t/T = 9.015$), the surface wave shape is essentially the same as shown in Figure (1). In Figure (2), the overall surface deformation effect of the nonlinear interactions is less than 4% of the wave amplitude in either direction. Over the duration of the simulation, the maximum difference between the superposed 2D waves and the 3D simulation was about 7% of the wave amplitude. However, at the end of the simulation, the nonlinear effects on the surface deformation were still increasing and would likely continue to increase for some time as resonant modes for the domain are excited (for a discussion of gravity wave resonance, see Phillips, 1974). If the simulation were continued, we expect

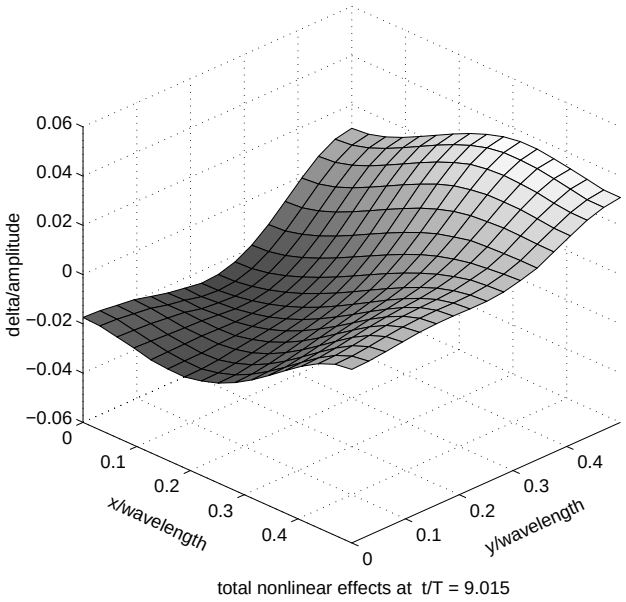

Figure 2: Total surface deformation (3D - superposed 2D)

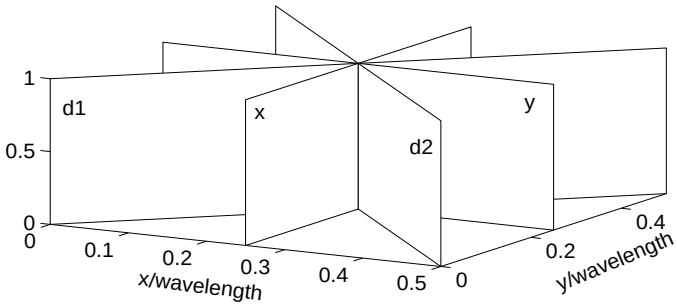

Figure 3: Symmetry/asymmetry planes

the nonlinear effects to eventually reach a zero growth rate or a stable oscillation as energy is exchanged between resonant wave modes.

To provide a better quantitative understanding and analysis of the nonlinear wave-wave interactions, we can decompose the total nonlinear effects (Figure 2) using symmetries and asymmetries around four cutting planes illustrated in Figure (3). These planes can be identified by the following axes:

- $d1$ — the main diagonal axis along which the overall sloshing is approximately symmetrical
- $d2$ — the secondary diagonal axis along which the overall sloshing is asymmetrical
- x — an axis where x/wavelength = 0.25
- y — an axis where y/wavelength = 0.25

The asymmetrical component of the surface deformation ($\Delta^{[a]}$) at a point (p) about a cutting plane (c_1) is defined as:

$$\Delta_p^{[a:c_1]} \equiv \frac{1}{2}\left(\eta_p - \eta_i^{[c_1]}\right) \tag{5}$$

where η_p is the surface deformation at point p, and $\eta_i^{[c_1]}$ is the surface deformation of the image point of p relative to the cutting plane c_1. The symmetrical component of the surface deformation ($\Delta^{[s]}$) is defined as:

$$\Delta_p^{[s:c_1]} \equiv \frac{1}{2}\left(\eta_p + \eta_i^{[c_1]}\right) \tag{6}$$

It follows that $\Delta_p^{[a:c_1]} + \Delta_p^{[s:c_1]} = \eta_p$. If we substitute $\Delta_p^{[s:c_1]}$ for η_p and the image point of $\Delta_p^{[s:c_1]}$ with respect to a second cutting plane (c_2) for $\eta_i^{[c_1]}$, then equations (5) and (6) become:

$$\left(\Delta_p^{[s:c_1]}\right)_p^{[a:c_2]} = \frac{1}{2}\left\{\Delta_p^{[s:c_1]} - \left(\Delta_p^{[s,c_1]}\right)_i^{[c_2]}\right\} \tag{7}$$

$$\left(\Delta_p^{[s:c_1]}\right)_p^{[s:c_2]} = \frac{1}{2}\left\{\Delta_p^{[s:c_1]} + \left(\Delta_p^{[s,c_1]}\right)_i^{[c_2]}\right\} \tag{8}$$

Using further recursions of equations (7) and (8) about each of the cutting planes decomposes the surface into sixteen components. The sum of the sixteen components is equal to the original

surface deformation. Fortunately, it turns out that only seven of the components are of any significance (with deformations larger than 0.1% of the wave amplitude). By recombining some of the seven significant components, five decomposed nonlinear effects can be defined:

1. Symmetry along both diagonal planes ($d1$ and $d2$) with asymmetry on the x and y planes (Figure 4).
2. Symmetry on only one diagonal plane (Figures 6 and 7).
3. Symmetry on all planes (Figure 9).
4. Symmetry on x and y planes, with asymmetry on both diagonal planes (Figure 10).

The first of these components (Figure 4) can be seen as two standing waves (one along each diagonal) with wavelengths equal to the the diagonal dimension of the domain. We will call this the "vertical velocity nonlinear effect" for reasons that will be apparent in due course. The second two effects (Figures 6 and 7) are diagonal sloshings with the longest wavelength equal to twice the diagonal dimension of the domain. The third and fourth effects are higher mode waves in the x and y directions that have wavelengths equal to the domain length. In the case of Figure (9), the higher mode waves are in phase so that their crests and troughs coincide in the center. In Figure (10), the higher mode waves are out of phase in the center of the domain.

To understand the development of the nonlinear effects, it is useful to examine a time history of the root-mean-square (RMS) of the deformation components. Figures (5), (8), and (11) provide this data for the various nonlinear terms. Note that the RMS graphs show two peaks for each period of a deformation component. However, in the case of the vertical velocity effect (Figure 5), the second peak is so small as to be almost non-existent.

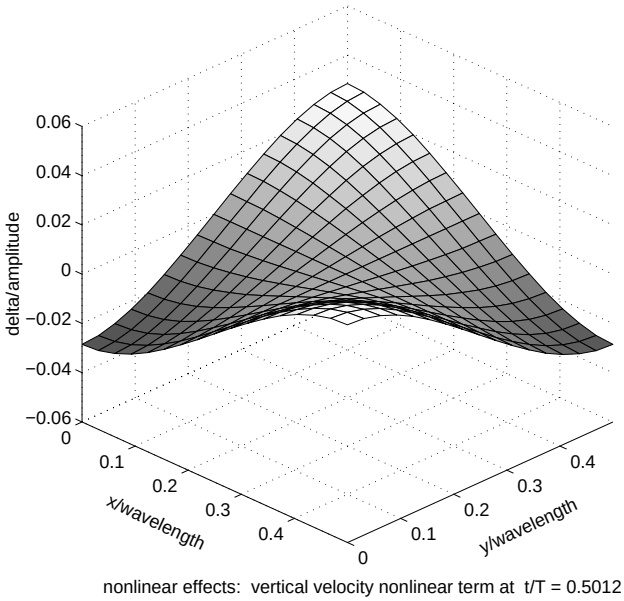

Figure 4: Symmetry across both diagonal planes

ANALYSIS

Vertical velocity nonlinear effect

Figures (4) and (5) provide the data for the "vertical velocity nonlinear effect." This component of the nonlinear effects has five major characteristics:

1. Unlike the other nonlinear effects, the oscillations of the vertical velocity effect are not symmetrical about the still free-surface level (the plane $delta = 0$ in Figure 4). In Figure (5), we see evidence of this in the large RMS peak followed by a very small (almost non-existent) peak. Figure (4) shows the shape of the vertical velocity effect at the top of a large peak. At the top of a small peak, the deformation effect is nearly flat, but is non-zero.
2. The effect shows no significant growth rate. This is consistent with the attribution of the effect to the vertical velocity. We would not expect to see large changes in the vertical velocity terms since such changes would require either rapid growth or rapid damping of the waves.
3. The frequency of the effect is approximately 1.25 times the frequency of the 2D wave, or about $7.33\,rad/sec$. This is in reasonable agreement with the theoretical value of $7.87\,rad/sec$ for a standing wave with a wavelength of the domain diagonal (which appears to be the longest wavelength in Figure 4).
4. This is initially the dominant nonlinear effect, but in the sixth period of the 3D wave combination, it is superseded by the nonlinear sloshing effects along the main diagonal ($d1$). By the eleventh period, the nonlinear sloshing effects along the minor diagonal ($d2$) are also larger than the vertical velocity effect (see Figure 8 for the sloshing effects).
5. In general, this effect shows a decrease in 3D free-surface height (relative to the combination of the 2D waves) at the corners of the main sloshing diagonal ($d1$) and an increase in height along the minor diagonal ($d2$) corners.

This phenomena is attributable to the Navier-Stokes' vertical velocity nonlinear term ($w\,\partial w/\partial z$, where w is the vertical velocity and z is the vertical coordinate). The nonlinear vertical velocity term is included in the superposed component waves, but its 3D effect is different from the sum of the effects of the

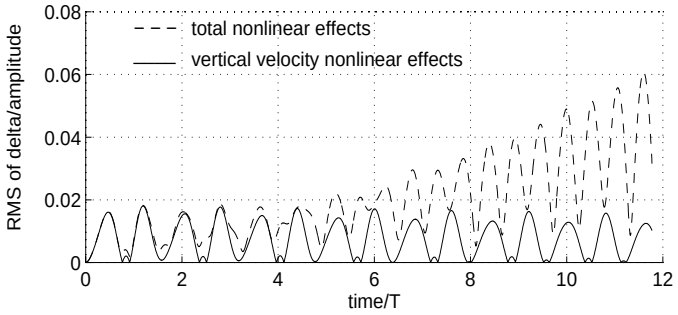

Figure 5: Vertical velocity surface deformation effects

2D component waves, since:

$$(w_1 + w_2)\frac{\partial}{\partial z}\Big(w_1 + w_2\Big) \neq w_1\frac{\partial w_1}{\partial z} + w_2\frac{\partial w_2}{\partial z} \qquad (9)$$

where the subscripts 1 and 2 indicate the monochromatic waves in the x and y directions, respectively. We note that if $w_1 = w_2$ then the nonlinear term on the left-hand side of equation (5) is twice as big as the nonlinear term on the right-hand side. Thus, if the velocity field is linearly superposed to the first order, then the vertical velocity nonlinear terms at the $d1$ corners of the 3D simulation will be approximately twice that of the superposed waves (or four times that of a single wave). For example, in the first half-period of the sloshing, along the vertical line at the corner $(0, 0, z)$ we have $w < 0$ and $\partial w/\partial z < 0$, while at the corner where $(0.5, 0.5, z)$ we have $w > 0$ and $\partial w/\partial z > 0$. It follows that in the Navier-Stokes equations, along the line of $(0, 0, z)$, the nonlinear term is accelerating the free surface downward; while along the line of $(0.5, 0.5, z)$, the nonlinear term is retarding the upward motion of the free surface. This is exactly the effect illustrated in Figure (4). Note that in the corners of the $d2$ diagonal the w_1 and w_2 terms are approximately equal and in opposite directions. Therefore, effect of the nonlinear term in the 3D simulation is close to zero, whereas the nonlinear terms in a superposition of the 2D simulations are of the same sign and will accumulate rather than cancel. Thus, the 3D simulation has less damping in the corners of the $d2$ diagonal than there is in the 2D nonlinear waves, resulting in the surface deformation effect being positive at these corners. Again, this is clearly shown in Figure (4).

Diagonal sloshing

Sloshing effects along the main ($d1$) and minor ($d2$) diagonals are illustrated in Figures (6), (7), and (8). The sloshing along the main diagonal exhibits the most rapid growth rate of any of the nonlinear effects. The frequency of the diagonal sloshings is approximately 0.94 times the frequency of the 2D wave, or about $5.5\,rad/sec$. While this is significantly greater than the theoretical value of $4.26\,rad/sec$ for a wavelength of twice the domain diagonal, it is qualitatively correct in that it shows a lower frequency than the 2D wave. Much as the primary 3D sloshing is composed of two 2D waves, each of the 3D nonlinear diagonal sloshing effects could be further decomposed into 2D waves in the x and y directions. Heuristically, one might expect the decomposed waves to follow the dispersion relation and oscillate at the same rate as the main sloshing. Therefore, it is significant that these components are oscillating at a slower rate than the primary sloshing. This indicates that the nonlinear effects are moving the system away from a superposition of two x and y waves, transforming it into a combination of waves along the $d1$ and $d2$ axes. Such waves have a longer primary wavelength and a lower frequency. It is obvious from Figure (8) that the nonlinear diagonal sloshing effects were still in a period of rapid change when the simulation was stopped. It is likely that a longer simulation would show a further decrease of the frequency and continued growth of the diagonal nonlinear terms.

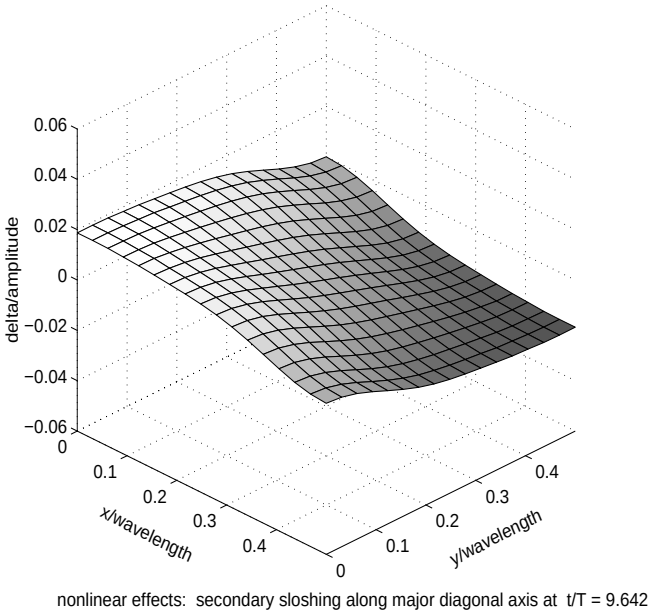

Figure 6: Symmetry along main diagonal

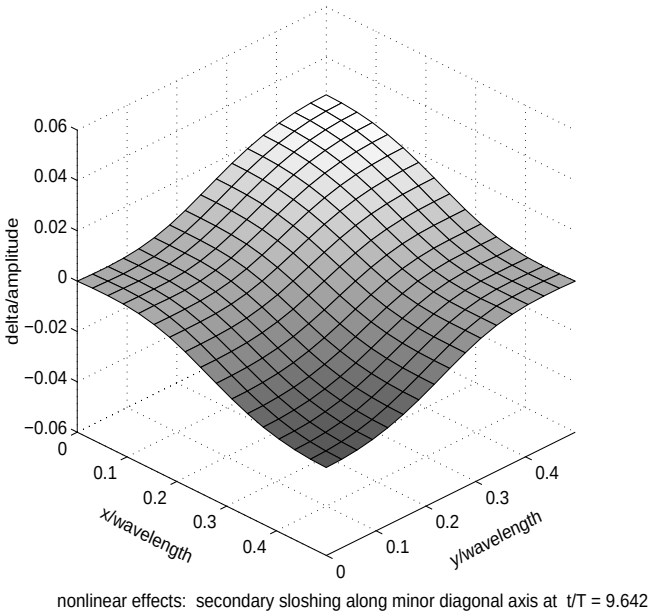

Figure 7: Symmetry along minor diagonal

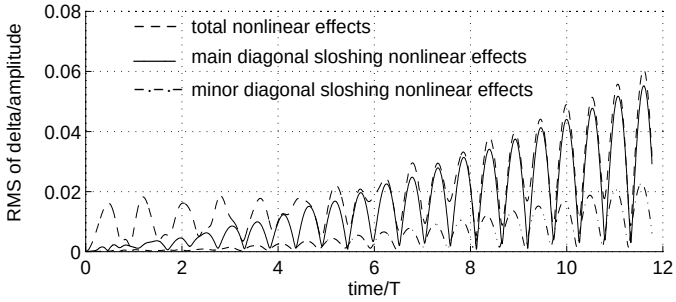

Figure 8: Diagonal sloshing surface deformation effects

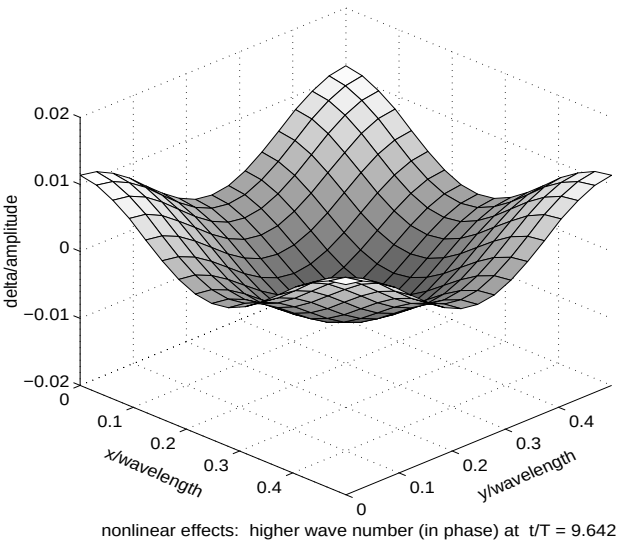

Figure 9: Symmetry with all planes

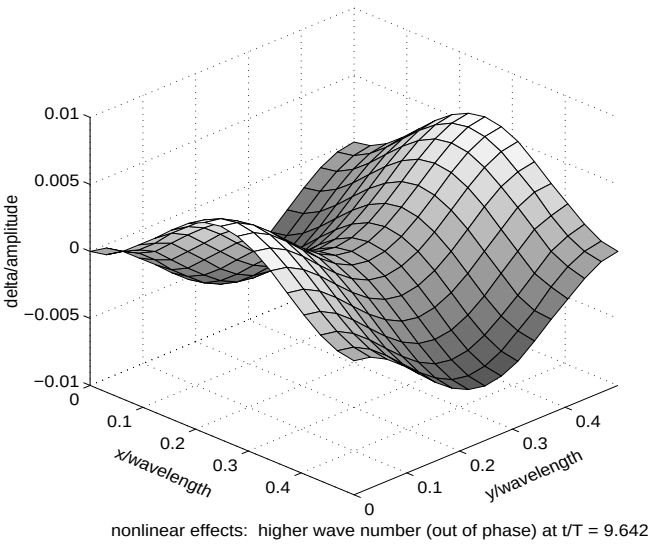

Figure 10: Symmetry with x and y planes

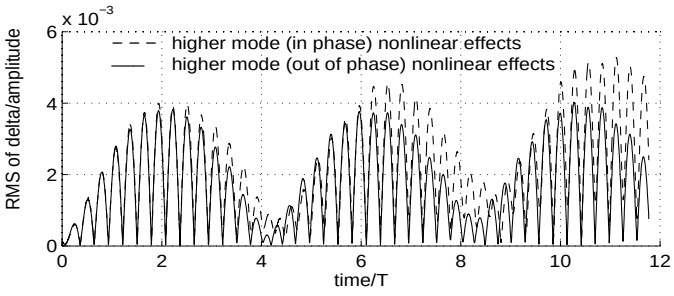

Figure 11: Higher mode surface deformation effects

Higher order modes

Surface deformations produced at higher modes in the x and y directions are illustrated in Figures (9) (10) and (11). These nonlinear effects are an order of magnitude smaller than the other effects and do not seem to have a significant growth rate. For all practical purposes, they play a very minor role in the wave interactions. It is interesting to note that Figure (11) shows the existence of several similar waves that are slightly out of phase so as to produce standing wave groups in the higher modes. This is probably due to reflection effects from the free-slip boundaries of the simulation.

Viscous effects

To analyze the viscous effects, we compare the maximum crest-to-trough wave height (as a function of time) to the viscous-damping theory of Lamb (1945), art. 348-349:

$$h(t) \;=\; h(0)\, e^{-2\nu k^2 t} \tag{10}$$

where $h\,(t)$ is the wave height as a function of time. Figure (12) shows the results for the 2D monochromatic sloshing, the 3D sloshing, and Lamb's theory. For purposes of comparison, the theory is shown for the k of the 2D superposed waves, as well as for the k for diagonal waves based upon the diagonal length and twice the diagonal length.

As shown in Figure (12), the 2D results are in excellent agreement with the theory, while 3D results and theory are in reasonable agreement, given that we are taking some liberties in applying the theory to the 3D case. Lamb's derivation is based on an energy argument for a steady, linear, 2D monochromatic wave which is characterized by a single wave number, while we are applying it to a nonlinear 3D case that has at least three significant wave numbers with effects that are time-dependent. Despite this, our results are fairly consistent with Lamb's theory. However, we should be careful not to attribute the entire

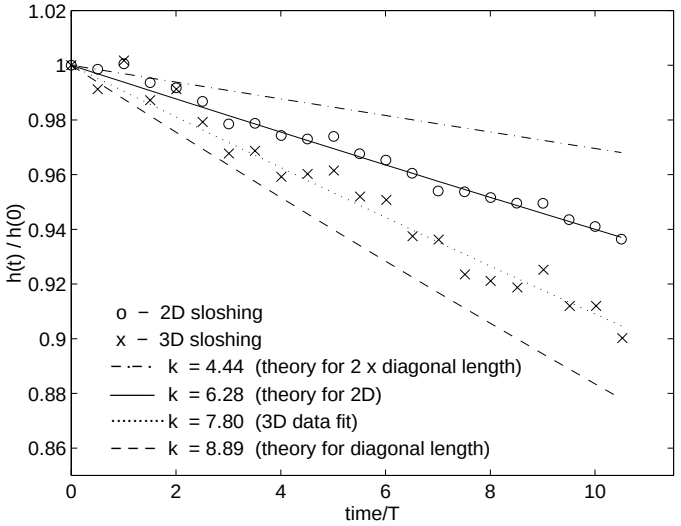

Figure 12: Change in maximum crest-to-trough height

change in the maximum wave height in the 3D simulation to viscous attenuation. A heuristic argument can be made that the individual deformation components should follow the damping theory and, therefore, the total damping should be the sum of the damping of the components. A brief review of the magnitudes of the nonlinear terms in Figures (5) and (8) and the difference in wave height between the 3D simulation and theory in Figure (12) shows that application of equation (10) to the nonlinear terms cannot account for all of the reduction in wave height. A better explanation is that a significant portion of the change in the wave height is caused by the nonlinear terms redistributing the wave energy away from the crests and troughs. For example, from Figure (7), the nonlinear sloshing effect along the minor diagonal ($d2$) has an amplitude of 3% of the combined wave amplitude. This alone could account for most of the difference between the damping theory and the 3D change in wave height.

CONCLUSION

This paper has demonstrated the ability of the numerical method to capture viscous and nonlinear effects in a 3D free-surface Navier-Stokes wave simulation. Comparisons have been made to the viscous damping theory of Lamb (1945) with reasonable agreement. The nonlinear wave-wave interactions have been decomposed into component effects that deform the 2D monochromatic waves of the initial conditions. Unfortunately, we have not found any laboratory experiments in the literature which would provide a suitable basis for direct validation of the 3D wave-wave interactions. This would perhaps be an interesting task that could provide a standard validation method for free-surface simulations, much as laboratory measurements of the lid-driven cavity flow have provided for turbulent flow simulations. We hope to provide further validation of the numerical method at a later date through simulations of progressive water waves and comparisons to laboratory data.

ACKNOWLEDGMENT

The support of the Fluid Dynamics Program, Mechanics and Energy Conversion Division, Office of Naval Research, through Grant N00014-94-1-0190 [Program Officer: Dr. E.Rood] is gratefully acknowledged.

REFERENCES

Borue, V., Orszag, S.A. and Staroselsky, I., 1995, "Interaction of surface waves with turbulence: direct numerical simulations of turbulent open-channel flow," *J. Fluid Mech.* Vol. 286, pp. 1-23.

Chan, R.K.-C., and Street, R.L., 1970, "SUMMAC - A numerical model for water waves," Technical Report 135, Stanford University, 155 pages.

Hodges, B.R., Street, R.L., and Zang, Y., 1994, "A method for simulation of viscous, non-linear, free-surface flows," *20th Symp. on Naval Hydrodynamics*, preprint volume W1 through Th5, pp. 247-265.

Hodges, B.R., 1996, *Numerical simulation of free-surface flows*, Ph.D. thesis, Department of Civil Engineering, Stanford University, Stanford, CA, to appear.

Kim, J., and Moin, P., 1985, "Application of a Fractional-Step Method to Incompressible Navier-Stokes Equations," *J. Comp. Physics*, Vol. 59, pp. 308-323.

Lamb, H., 1945, *Hydrodynamics*, 6th ed., Dover Publications.

Phillips, O.M., 1974, "Wave Interactions," in *Nonlinear Waves*, ed. S. Leibovich and A.R. Seebass, Cornell University Press, pp. 186-211.

Wiegel, R.L., 1964, *Oceanographical Engineering*, Prentice-Hall, Inc.

Zang, Y., Street, R.L. and Koseff, J.R., 1994 "A Non-staggered Grid, Fractional Step Method for Time-Dependent Incompressible Navier-Stokes Equations in Curvilinear Coordinates," *J. Comp. Physics*, Vol. 114, pp. 18-33.